

Haverford College

Haverford Scholarship

Faculty Publications

Astronomy

2011

FIRE Spectroscopy of the Ultra-Cool Brown Dwarf, UGPS J072227.51–054031.2: Kinematics, Rotation, and Atmospheric Parameters

John J. Bochanski

Haverford College, jbochans@haverford.edu

Adam J. Burgasser

Robert A. Simcoe

Andrew A. West

Follow this and additional works at: https://scholarship.haverford.edu/astronomy_facpubs

Repository Citation

John J. Bochanski, Adam J. Burgasser, Robert A. Simcoe, and Andrew A. West. "FIRE Spectroscopy of the Ultra-Cool Brown Dwarf, UGPS J072227.51–054031.2: Kinematics, Rotation, and Atmospheric Parameters." *The Astronomical Journal* 142 (4): 169. 2011.

This Journal Article is brought to you for free and open access by the Astronomy at Haverford Scholarship. It has been accepted for inclusion in Faculty Publications by an authorized administrator of Haverford Scholarship. For more information, please contact nmedeiro@haverford.edu.

FIRE SPECTROSCOPY OF THE ULTRA-COOL BROWN DWARF, UGPS J072227.51–054031.2: KINEMATICS, ROTATION AND ATMOSPHERIC PARAMETERS*

JOHN J. BOCHANSKI^{1,2}, ADAM J. BURGASSER^{2,3,6}, ROBERT A. SIMCOE^{2,7}, AND ANDREW A. WEST^{4,5,8}

¹ Astronomy and Astrophysics Department, Pennsylvania State University, 525 Davey Laboratory, University Park, PA 16802, USA; jjb29@psu.edu

² Kavli Institute for Astrophysics and Space Research, Massachusetts Institute of Technology, Building 37, 77 Massachusetts Avenue, Cambridge, MA 02139, USA

³ Center for Astrophysics and Space Science, University of California San Diego, La Jolla, CA 92093, USA

⁴ Department of Astronomy, Boston University, 725 Commonwealth Avenue, Boston, MA 02215, USA

⁵ Department of Terrestrial Magnetism, Carnegie Institution of Washington, 5241 Broad Branch Road, NW, Washington, DC 20015, USA

Received 2011 July 29; accepted 2011 September 12; published 2011 October 17

ABSTRACT

We present $\lambda/\Delta\lambda \sim 6000$ near-infrared spectroscopy of the nearby T9 dwarf, UGPS J072227.51–054031.2, obtained during the commissioning of the Folded-Port Infrared Echellette Spectrograph on the Baade Magellan telescope at Las Campanas Observatory. The spectrum is marked by significant absorption from H_2O , CH_4 , and H_2 . We also identify NH_3 absorption features by comparing the spectrum to recently published line lists. The spectrum is fit with BT-Settl models, indicating $T_{\text{eff}} \sim 500\text{--}600$ K and $\log g \sim 4.3\text{--}5.0$. This corresponds to a mass of $\sim 10\text{--}30 M_{\text{Jup}}$ and an age of 1–5 Gyr, however, there are large discrepancies between the model and observed spectrum. The radial and rotational velocities of the brown dwarf are measured as 46.9 ± 2.5 and 40 ± 10 km s^{−1}, respectively, reflecting a thin disk Galactic orbit and fast rotation similar to other T dwarfs, suggesting a young, possibly planetary-mass brown dwarf.

Key words: brown dwarfs – infrared: stars – stars: fundamental parameters – stars: individual (UGPS J072227.51–054031.2) – stars: kinematics and dynamics – stars: low-mass

Online-only material: color figures

1. INTRODUCTION

Late-type T dwarfs ($T < 600$ K) are among the dimmest, coldest, and least massive products of star formation. As cooling brown dwarfs (BDs), these objects sample a broad range of age and mass, from old, relatively massive relics of the earliest epochs of Galactic star formation to recently formed planetary-mass objects incapable of deuterium fusion ($M < 13 M_{\text{Jup}}$; Burrows et al. 2001). Their numbers in the vicinity of the Sun help constrain the substellar initial mass function (e.g., Metchev et al. 2008; Burningham et al. 2010) and the minimum formation mass (e.g., Burgasser 2004). Late-type T dwarfs also occupy the same physical parameter space (mass, age, T_{eff}) as exoplanets, with moderate separations (0.5–1 AU) from solar-type stars, making them important benchmarks of exoplanet models (i.e., Burrows et al. 1997; Baraffe et al. 2003) and direct detection experiments (i.e., Macintosh et al. 2006).

Despite its astronomical utility, high-resolution spectroscopy of late T dwarfs is exceedingly rare. The main culprit is faint T dwarf luminosity ($L \sim 2 \times 10^{-6} L_{\odot}$ for T9; Golimowski et al. 2004). Recently, surveys such as the *Wide-field Infrared Survey Explorer* (WISE; Wright et al. 2010) and the UKIRT Infrared Deep Sky Survey (UKIDSS; Lawrence et al. 2007) have produced deep multi-band photometry over thousands of square degrees in the near-infrared (NIR; $\sim 1\text{--}2.5 \mu\text{m}$) and mid-IR ($\sim 3\text{--}5 \mu\text{m}$), yet many of the cool T dwarfs discovered in these surveys have been studied at low spectral resolutions ($R = \lambda/\Delta\lambda < 1000$), blending rich absorption bands produced by CH_4 , NH_3 , and H_2O and complicating their atmospheric analyses.

These low-resolution observations also limit the precision of radial and rotational velocity measurements. Higher resolution observations are only feasible for bright objects, biasing their kinematic analysis to the nearby BD population. For example, the largest study of T dwarfs with measured rotation velocities contained only nine objects (Zapatero Osorio et al. 2006).

Currently, there are <20 BDs classified as T9 or later. One of the brightest of these sources is UGPS J072227.51–054031.2 (hereafter UGPS 0722–05), discovered in the UKIDSS data by Lucas et al. (2010), and tentatively assigned a spectral type of T10 based on its strong molecular absorption and faint absolute magnitude. The spectral type of UGPS 0722–05 was revised by Kirkpatrick et al. (2011) and Cushing et al. (2011) to T9 and it has been designated as the infrared spectral standard. UGPS 0722–05 is a tantalizing target for follow-up studies, as it is relatively nearby ($d \sim 4.1$ pc; see Table 1) and bright ($J = 16.5$). In this paper, we present a moderate resolution ($R \sim 6000$) NIR spectrum of UGPS 0722–05, acquired using the newly installed Folded-Port Infrared Echellette Spectrograph (FIRE; Simcoe et al. 2010). The observations are detailed in Section 2. In Section 3, the NIR spectral energy distribution and corresponding model fits are shown along with the rotational and radial velocities and Galactic orbit of UGPS 0722–05. Finally, our conclusions and paths for future investigations are presented in Section 4.

2. FIRE OBSERVATIONS AND REDUCTIONS

The FIRE spectrograph (Simcoe et al. 2008, 2010) was installed and commissioned on the Magellan Baade telescope at Las Campanas Observatory during 2010 March and April. FIRE is a single-object spectrograph with two modes: a cross-dispersed echellette mode with moderate resolution ($R \sim 6000$) and a long-slit low-resolution mode ($R \sim 250\text{--}350$). The spectrum is imaged on a HAWAII-2RG chip, with continuous

* This paper includes data gathered with the 6.5 m Magellan Telescopes located at Las Campanas Observatory, Chile.

⁶ Hellman Fellow.

⁷ Sloan Fellow.

⁸ Visiting Investigator.

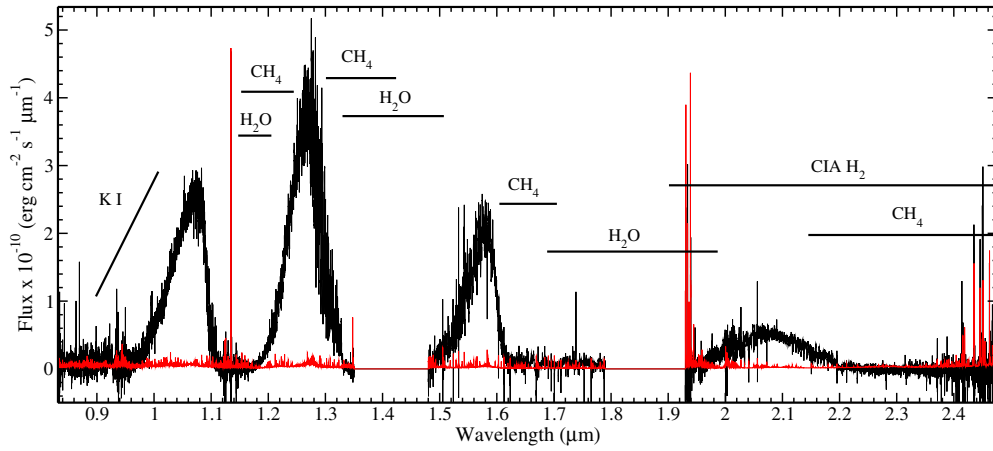


Figure 1. FIRE spectrum of UGPS 0722–05 (black line). The noise spectrum is shown in red. Major atomic and molecular absorption features are labeled. Note the strong CH₄ absorption, indicative of a cool T dwarf. Strong telluric absorption between bands has been masked.

(A color version of this figure is available in the online journal.)

Table 1
Measured Properties of UGPS 0722–05

Property	Value	Source ^a
α (J2000)	07:22:27.51	1
δ (J2000)	−05:40:31.2	1
μ_α (mas yr ^{−1})	−910 ± 8	1
μ_δ (mas yr ^{−1})	1020 ± 3	1
π (mas)	237 ± 41	1
RV (km s ^{−1})	46.9 ± 2.5	2
v_{tan} (km s ^{−1})	19 ± 4	1
$v \sin i$ (km s ^{−1})	40 ± 10	2
V_R (km s ^{−1})	−42 ± 2	2 ^b
V_ϕ (km s ^{−1})	221 ± 1	2 ^b
V_Z (km s ^{−1})	4 ± 1	2 ^b
i	24.80 ± 0.13	1
z	20.51 ± 0.09	1 ^c
Y	17.37 ± 0.02	1
J	16.52 ± 0.02	1
H	16.90 ± 0.02	1
K	17.07 ± 0.08	1
[3.6]	14.28 ± 0.05	1
[4.5]	12.19 ± 0.04	1
W_1	15.15 ± 0.05	4
W_2	12.17 ± 0.03	4
W_3	10.18 ± 0.06	4
Spectral Type	T9	3
T_{eff}	500–600 K	2
$\log g$	4.2–5.0	2
Mass	10–30 M_{Jup}	2
Age	1–5 Gyr	2

Notes.

^a 1: Lucas et al. (2010), 2: This Paper, 3: Cushing et al. (2011), 4: Wright et al. (2010).

^b Computed using the solar velocity of Schönrich et al. (2010).

^c Average of two z reported values.

coverage from 0.85 to 2.5 μm . In the cross-dispersed mode, the spectrum is spread over 21 orders, with some overlap in wavelength coverage at the edges of each order. Target acquisition is achieved with a second NIR imager and Mauna Kea Observatory J filter focused on the entrance slit. FIRE was designed to be sensitive, employing the latest generation of HgCdTe detectors while limiting the number of reflective and transmissive surfaces, resulting in a zero point of ~ 16 mag (for 1 count pixel^{−1} s^{−1} across JHK) for the echelle mode.

On 2010 April 6 UT, we obtained four 900 s exposures of UGPS 0722–05 in FIRE’s echelle mode. The sky was clear with no cloud cover, and seeing was $\sim 0''.5$ in J at the time of observation. The $0''.6$ slit was used and aligned with the parallactic angle and the air mass was 1.4. The exposures were dithered along the slit in an ABBA dither pattern and a Fowler sampling of 8 was employed. An A0V star, HIP 63714, was observed for telluric correction and flux calibration purposes. Quartz flat fields and thorium–argon (ThAr) arcs were obtained after the science and telluric calibrator exposures.

The images were reduced using the FIRE reduction software package, FIREHOSE, which is based on the MASE pipeline (Bochanski et al. 2009) for the MagE spectrograph (Marshall et al. 2008). FIREHOSE, like MASE, was designed to reduce cross-dispersed echelle spectra with curved orders. Quartz lamp images were used to identify the order boundaries and derive flat-field and illumination corrections. A combination of OH telluric lines and ThAr arc images were used to determine the wavelength solution along the center of each order and its tilt in the spatial direction, which was used to construct a two-dimensional vacuum wavelength map. The typical uncertainty of the wavelength solution was 0.15 pixels, corresponding to 0.04–0.4 Å depending on the order. A two-dimensional sky model was constructed using basis splines (Kelson 2003) and subtracted from each order. This step eliminates the need for ABBA-type dithers for sky subtraction.⁹ An optimal extraction routine was then performed on each order (Horne 1986), extracting the object flux onto a heliocentric rest-frame wavelength grid. Telluric corrections were incorporated into the pipeline using a modified version of *xtellcor* from Spextool (Cushing et al. 2004; Vacca et al. 2003). Telluric absorption was quantified by comparing the telluric stellar spectrum to a model Vega spectrum reddened using the $B-V$ color of HIP 63714, velocity shifted, and broadened using the 1.005 μm H 1 Pa δ line as a line kernel. The science target was also flux-calibrated during this step. Multiple spectra of the same target were combined after flux calibration. Finally, the extracted orders were combined into a one-dimensional spectrum, with overlap regions averaged together. The final spectrum is shown in Figure 1. The peak signals to noise in the y , J , H , and K bands are ~ 250 , 350, 200, and 60 respectively. As a test of the flux calibration and telluric

⁹ However, for faint sources, multiple exposures are still needed to avoid saturating sky lines.

Table 2
Radial Velocity Measurements

Standard	RV (km s ⁻¹)	Notes ^a
$T = 400$ K	47.9	BT-Settl model from Allard et al. (2010)
$T = 500$ K	49.2	BT-Settl model from Allard et al. (2010)
$T = 600$ K	48.5	BT-Settl model from Allard et al. (2010)
$T = 700$ K	48.5	BT-Settl model from Allard et al. (2010)
2M0415–0935	45.6	Assuming 49.6 km s ⁻¹ for template (Zapatero Osorio et al. 2007)
2M0559–1404	46.8	Assuming –13.8 km s ⁻¹ for template (Zapatero Osorio et al. 2007)
2M1553+1532	41.8	Assuming –32.9 km s ⁻¹ for template (Zapatero Osorio et al. 2007)
Mean RV	46.9	2.5 km s ⁻¹ uncertainty

Note.

^a All RV measurements were computed in the J band from 1.27 to 1.31 μm .

correction, we computed synthetic $J-H$ and $H-K$ colors from the final spectrum, and compared them to the measured values reported in Table 1. The $J-H$ color agreed within 0.1 mag, while $H-K$ differed by ~ 0.5 mag, indicating the overall flux calibration between orders is sufficient for spectral analysis.

3. RESULTS

3.1. Spectral Properties

Since the FIRE spectrum of UGPS 0722–05 is the highest resolution observation of one of the coolest BDs, we compiled the most recent laboratory line lists for H_2O , CH_4 , and NH_3 to identify absorption features (Barber et al. 2006; Nassar & Bernath 2003; Yurchenko et al. 2011, respectively). The HITRAN 2008 database was also used to supplement the line lists (Rothman et al. 2009). Prior to comparing to the FIRE spectrum of UGPS 0722–05, each line list was cropped to 0.8–2.5 μm and smoothed with a 50 km s⁻¹ Gaussian kernel, which corresponds to one FIRE resolution element. The absorption intensities for each line list (in units of cm molecule⁻¹) were scaled by the relative molecular abundances shown in Figure 3 of Saumon et al. (2006) for $T_{\text{eff}} = 500$ K. The non-equilibrium abundances were assumed for NH_3 . The scaled values were then plotted along with the UGPS 0722–05 spectrum, and molecular features were manually identified. An example of our line list comparisons is shown in Figure 2.

In Figure 3, we plot expanded views of the UGPS 0722–05 spectrum in the y , J , H , and K bands. Prominent absorption features are labeled in each panel. Of note in Figure 3 is the significant number of absorption features throughout the spectrum that are attributed to H_2O , CH_4 , and NH_3 . There are a large number of blends between the molecular features, especially with H_2O , but some isolated absorption bands do exist. We confirm the tentative identification of NH_3 by Lucas et al. (2010) near 1.514 μm . Additional isolated NH_3 absorption features can be found near 1.234, 1.244, 1.52, 1.526, 1.542, 1.56, 1.566, 1.568, and 1.574 μm . This suggests that observations spanning 1.5–1.6 μm present the best chance at directly detecting NH_3 at these temperatures. While the detection of NH_3 has been suggested as the hallmark of the Y spectral class (i.e., Leggett et al. 2007), these weak features are consistent with the end of the T dwarf sequence as advocated by Cushing et al. (2011).

CH_4 exhibits prominent absorption bands near 1.6 and 2.15 μm . The structure seen in the UGPS 0722–05 spectrum is usually not detected at lower resolutions. These features may be used to derive spectral indices and provide isolated regions of the spectrum to derive atmospheric parameters (see Section 3.4).

3.2. Radial Velocity

The resolution of FIRE’s echelle mode permits the measurement of UGPS 0722–05’s radial velocity (RV) with a precision of a few km s⁻¹. We cross-correlated the spectrum of UGPS 0722–05 against other T dwarfs observed with FIRE and model atmosphere predictions. The T dwarf RV standards (Table 2) were taken from Zapatero Osorio et al. (2007) and were observed with a similar setup on FIRE as part of a larger effort to quantify BD kinematics (A. J. Burgasser et al. 2011, in preparation). We also employed the $T = 400$ K, 500 K, 600 K, and 700 K models (with $\log g = 5.0$, $[m/\text{H}] = 0.0$) from the BT-Settl grid (Allard et al. 2010). The 1.27–1.31 μm spectral region in the J band contains many strong molecular features, making it ideal for cross-correlation. The models were smoothed to match the resolution of the FIRE observations. Cross-correlations were computed using the *xcorl* IDL routine (Basri & Martín 1999; Mohanty & Basri 2003; West & Basri 2009). The reported RV and uncertainty were computed by taking the unweighted mean and the standard deviation of the individual RV measurements, respectively. The measured RV and uncertainty for UGPS 0722–05 is 46.9 ± 2.5 km s⁻¹.

3.2.1. Galactic Orbit

To frame the kinematics of UGPS 0722–05 in a Galactic context, we computed its orbit using its measured velocity and position as initial conditions. Using the distance, position, proper motion, and RV reported in Table 1, we computed the cylindrical velocity vector $[V_R, V_\phi, V_Z]$ where the local standard of rest is $[0, 220, 0]$ km s⁻¹ (Kerr & Lynden-Bell 1986), the solar motion is $[11.1, 12.24, 7.25]$ km s⁻¹ (Schönrich et al. 2010), and the RV component V_R increases in the direction of the Galactic center (Johnson & Soderblom 1987). The Sun’s radial position (X) was taken to be 8.5 kpc away from the Galactic center (Kerr & Lynden-Bell 1986) and 27 pc above the plane (Z; Chen et al. 2001; Jurić et al. 2008). Note that we are reporting velocities in a Galactocentric frame, rather than the traditional heliocentric UVW frame. While the effect is negligible for UGPS 0722–05, using UVW rather than a Galactocentric frame can introduce errors of a few km s⁻¹ for distances $\gtrsim 100$ pc. Employing a Galactocentric velocity frame will be important as more distant dwarfs are discovered in the next generation of surveys (i.e., the Large Synoptic Survey Telescope).

The orbit was integrated assuming a set of static, spherically symmetric oblate Plummer’s sphere potentials for the Galactic halo, bulge, and disk, using the forms described in Kuzmin (1956) and Miyamoto & Nagai (1975) and with parameters from Daiphole & Colin (1995). A Runge–Kutta integrator was

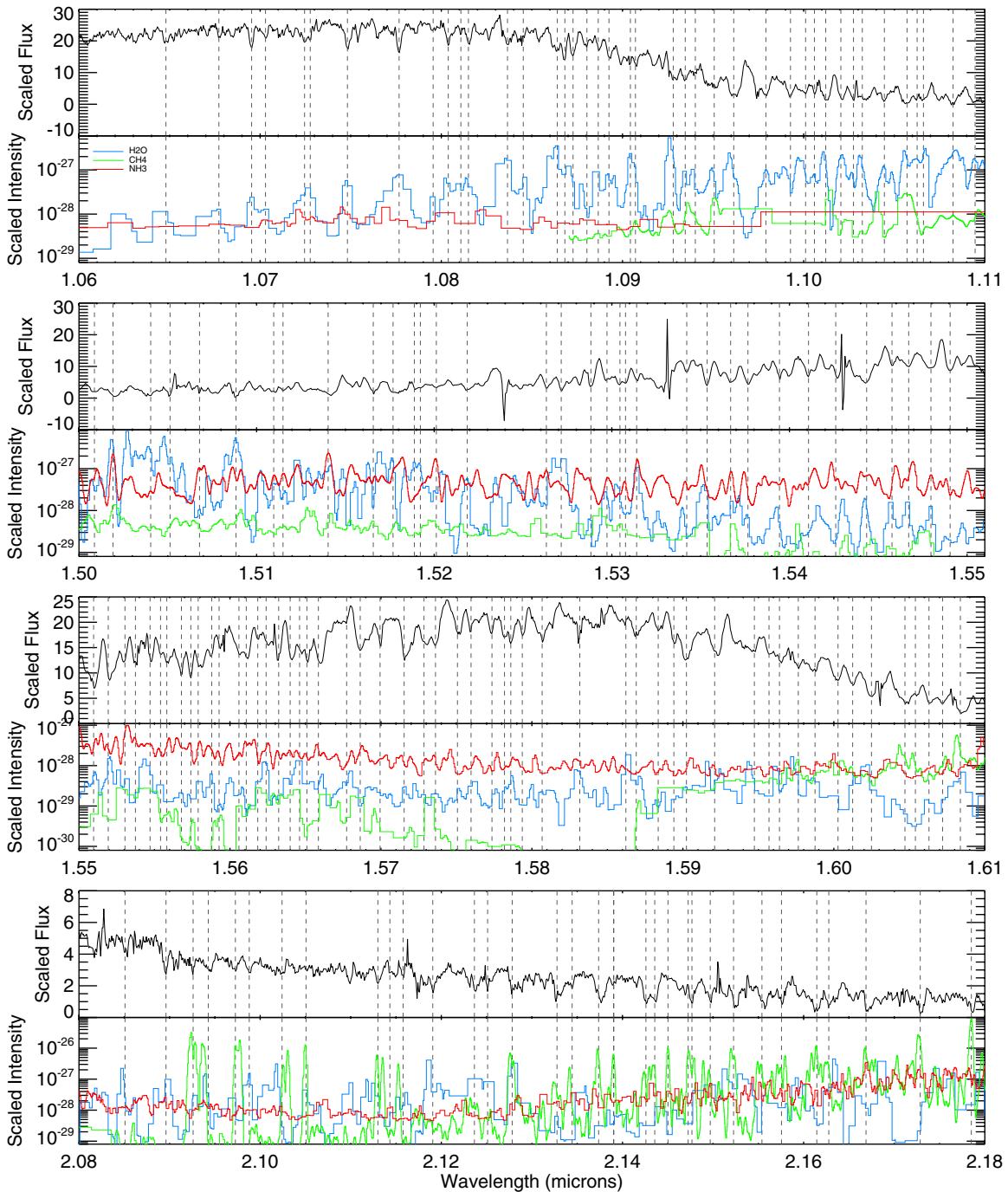


Figure 2. Comparison of UGPS 0722–05’s spectrum (black line) to molecular line lists (NH₃: red line, CH₄: green line, H₂O: blue line). The absorption intensity (cm molecule^{−1}) was scaled by the relative abundances for each molecule at $\log T = 2.7$ (from Saumon et al. 2006). Absorption features detected in both the spectrum of UGPS 0722–05 and the molecular absorption intensity spectra are marked by vertical dashed lines.

(A color version of this figure is available in the online journal.)

used to calculate the orbit over a period of ± 250 Myr with a 10 kyr time step, and both energy and the Z-component of angular momentum were conserved to better than one part in 10^5 . To sample measurement uncertainties in the distance and velocity of UGPS 0722–05 relative to the Sun, we computed 100 realizations of the orbit through the Monte Carlo method, varying the starting conditions assuming normal distributions with means and widths given by the values in Table 1.

The baseline calculation is shown in Figure 4, revealing a flat orbit with small eccentricity (e). The maximum vertical dis-

placement of the source from the Galactic plane never exceeds $Z \sim 60$ pc, with radial excursions between $7 \text{ kpc} < R < 9.5 \text{ kpc}$, and $e = 0.11 \pm 0.02$. This orbit is consistent with membership in the Galactic thin disk population (Bochanski et al. 2007) suggesting that UGPS 0722–05 is a relatively young BD. However, we strongly caution the use of kinematic properties as an age discriminant, as they should only be considered in a statistical manner. Computing orbits for larger samples of MLTY dwarfs will help place the orbit of UGPS 0722–05 in a broader context.

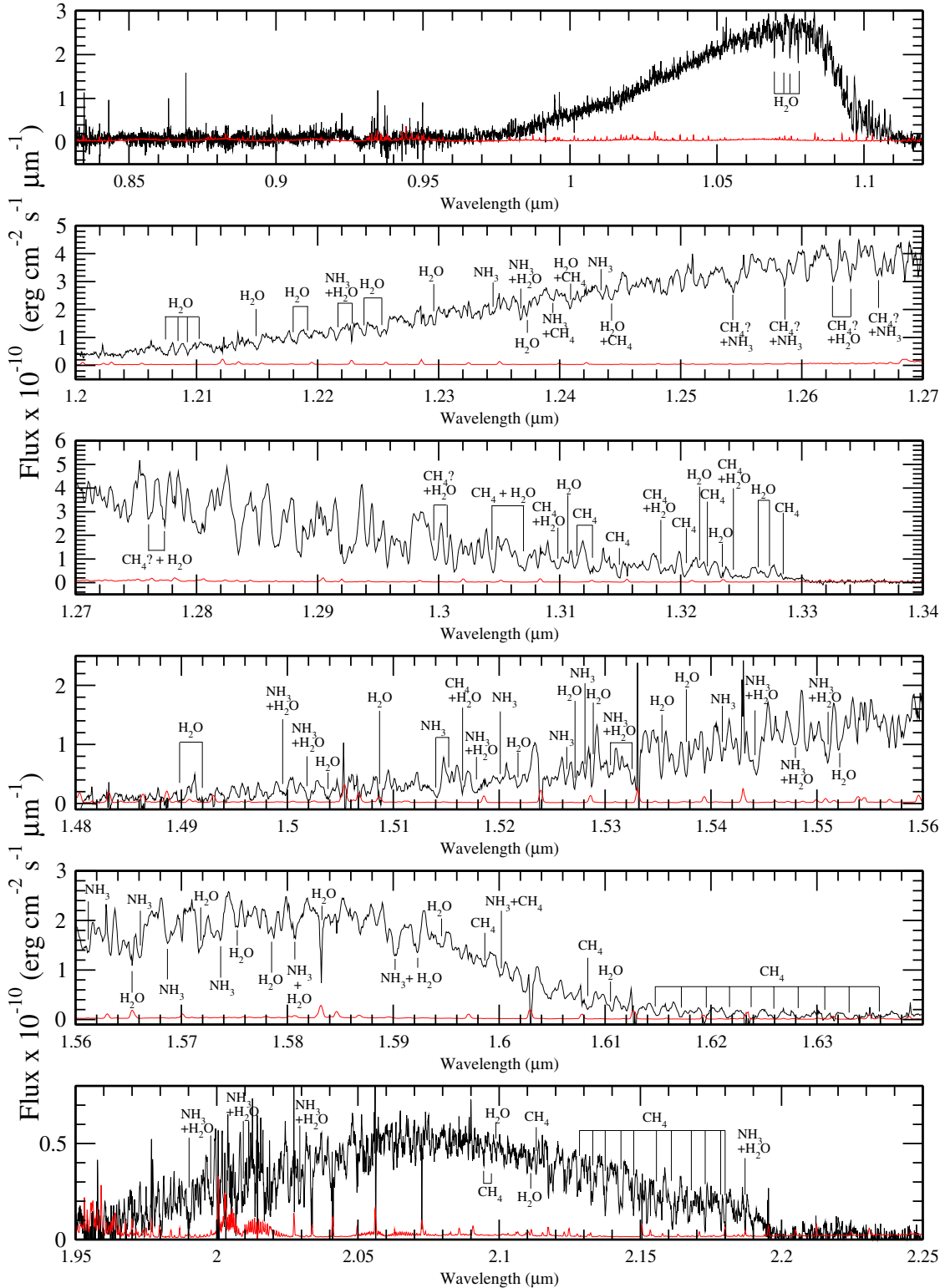


Figure 3. FIRE spectrum of UGPS 0722–05 (black line). The noise spectrum is shown in red. Major molecular features are labeled. Some CH₄ features are labeled with a “?” indicating regions where line lists are incomplete, but strong methane absorption has been observed (Fink & Larson 1979).

(A color version of this figure is available in the online journal.)

3.3. Rotational Velocity

The rotational velocity of UGPS 0722–05 was also measured with a technique used by a number of previous studies (e.g., Reid & Mahoney 2000; Mohanty & Basri 2003; West & Basri

2009). Briefly, the science object (UGPS 0722–05) is cross-correlated with a rotationally unbroadened template (the $T = 500$ K, $\log g = 5.0$ model, $[m/H] = 0.0$ from BT-Settl; Allard et al. 2010). The model is convolved with a Gaussian of 50 km s^{-1} to approximate the effects of FIRE’s line-spread

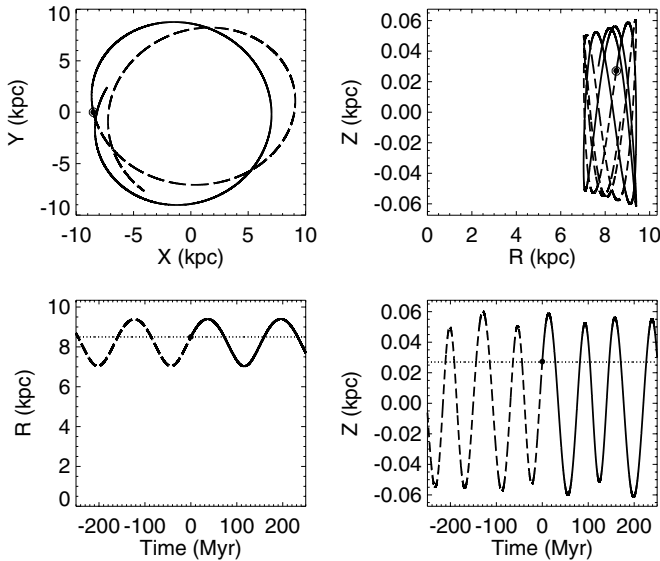


Figure 4. Simulated orbit of UGPS 0722–05. The object maintains a low eccentricity thin disk orbit over the length of the simulation. The radial excursions of UGPS 0722–05 are ~ 1 kpc, while the object maintains a vertical displacement of $\lesssim 60$ pc away from the Galactic plane.

function. This cross-correlation function (CCF) is compared to the CCFs derived from correlating the unbroadened template to rotationally broadened versions of itself. We constructed a series of rotating templates ranging in $v \sin i$ from 10 to 120 km s^{-1} , in steps of 10 km s^{-1} using the technique described in Gray (1992). In Figure 5, we compare the autocorrelation of the template against the CCFs of the $v \sin i = 30, 40$, and 60 km s^{-1} templates and the CCF of UGPS 0722–05 over the same wavelength range described in Section 3.2. While $v \sin i = 40 \text{ km s}^{-1}$ was the closest match to the CCF of UGPS 0722–05, the $v \sin i = 30$ and 50 km s^{-1} were good fits to most of the CCF trough (see Figure 5). Thus, we report a $v \sin i$ for UGPS 0722–05 is $40 \pm 10 \text{ km s}^{-1}$.

This rotation velocity is similar to those of late L and T dwarfs (e.g., Zapatero Osorio et al. 2006; Reiners & Basri 2008). Of the nine T dwarfs observed by Zapatero Osorio et al. (2006), only one BD (SDSSJ134646.45–003150.4) had a $v \sin i$ under 20 km s^{-1} and the authors speculated that this may be due to inclination.¹⁰ The remaining eight T dwarfs demonstrated rotational velocities between 20 and 40 km s^{-1} and this distribution does not vary significantly from the observed rotation velocities of L dwarfs (Reiners & Basri 2008). The $v \sin i$ of UGPS 0722–05 reinforces the findings of previous studies suggesting that T dwarfs are inefficient at rotational braking. In solar-type stars, magnetic fields power two sources of angular momentum loss: disk braking and flaring events (Skumanich 1972; Bouvier et al. 1997). Large-scale magnetic fields can form in convective, rotating low-mass objects (i.e., Browning 2008) and have been observed in some late M and L dwarfs (Reiners & Basri 2008; Hallinan et al. 2008), but remain undetected in T dwarfs (Berger 2006). This may indicate the lack of magnetic fields in T dwarfs, or alternatively, a weak coupling between the fields and the predominately neutral atmosphere. This de-coupling would reduce disk braking and flare frequency

¹⁰ Using the binomial function formalism from Browning et al. (2010), there is a $\sim 72\%$ chance of observing one slow rotator ($< 20 \text{ km s}^{-1}$) in a sample of nine stars, assuming that they all rotate at 40 km s^{-1} .

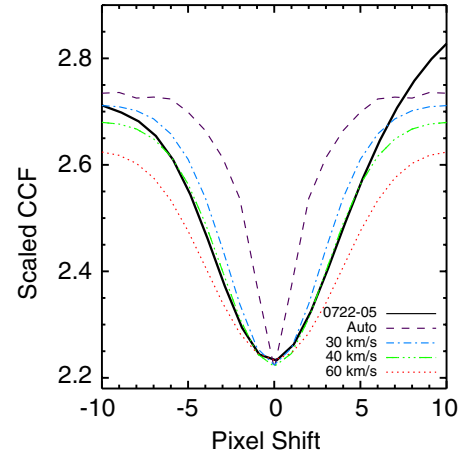


Figure 5. Cross-correlation functions of the broadened $T = 500$ K models. The purple dashed line corresponds to the autocorrelation function, the blue dash-dot line is the $v \sin i = 30 \text{ km s}^{-1}$ template, the green dot-dot-dash line is the $v \sin i = 40 \text{ km s}^{-1}$ template, and the red dotted line is the $v \sin i = 60 \text{ km s}^{-1}$ template. The CCF of UGPS 0722–05 with the unbroadened template is the solid black line. The CCFs have been shifted and scaled to match at the minimum. It is evident that there is some noticeable rotation, as the autocorrelation function is narrow compared to the observation. In contrast, the $v \sin i = 60 \text{ km s}^{-1}$ is too wide. We report the $v \sin i$ of UGPS 0722–05 as $40 \pm 10 \text{ km s}^{-1}$.

(A color version of this figure is available in the online journal.)

(due to reconnection events), which would decrease angular momentum loss in T dwarfs compared to solar-type stars.

3.4. Atmospheric Model Fits

To examine the physical properties of UGPS 0722–05, we compared its FIRE spectrum to the BT-Settl models of Allard et al. (2010). These models are based on the PHOENIX code (Hauschildt et al. 1999), and reflect an update to the original Settl models of Allard et al. (2003) with a microturbulence velocity field determined from two-dimensional hydrodynamic models (Freytag et al. 2010) and updated solar abundances from Asplund et al. (2009). We adopted a set of solar-metallicity ($[M/H] = 0.0$) models sampling $T_{\text{eff}} = 400\text{--}900$ K in 100 K steps, and $\log g = 3.5\text{--}5.5 \text{ cm s}^{-2}$ in 0.5 cm s^{-2} steps, with the exceptions that violate evolutionary parameters (e.g., $T_{\text{eff}} \leq 700$ K and $\log g = 5.5$).

Our fitting procedure was based on the formalism developed by Cushing et al. (2008), Bowler et al. (2009) and Burgasser et al. (2010). Model surface fluxes (in f_{λ} units) were smoothed to a common resolution of $\lambda/\Delta\lambda = 6000$ using a Gaussian kernel, and both models and FIRE data were interpolated onto a common wavelength grid spanning 0.9–2.4 μm . The FIRE data were also scaled to the observed J magnitude of UGPS 0722–05. We then performed eight separate fits to the data, encompassing the full spectral range (excluding regions of strong telluric absorption), the $yJHK$ spectral peaks, and three “narrow” regions (0.04–0.12 μm in width) sampling strong molecular absorption (Table 3). Data and models were compared using a χ^2 statistic, with the degrees of freedom equal to the number of resolution elements sampled. The optimal scaling factor minimizing χ^2 was computed following Cushing et al. (2008) and is equivalent to $(R/d)^2$, where R is the radius of the BD and d its distance from the Sun (Bowler et al. 2009). Two sets of fits were done, one in which the distance was treated as a free parameter and one in which the model-derived distance must agree with the parallax measurement of Lucas et al. (2010) to within 5σ . We also allowed for variations in

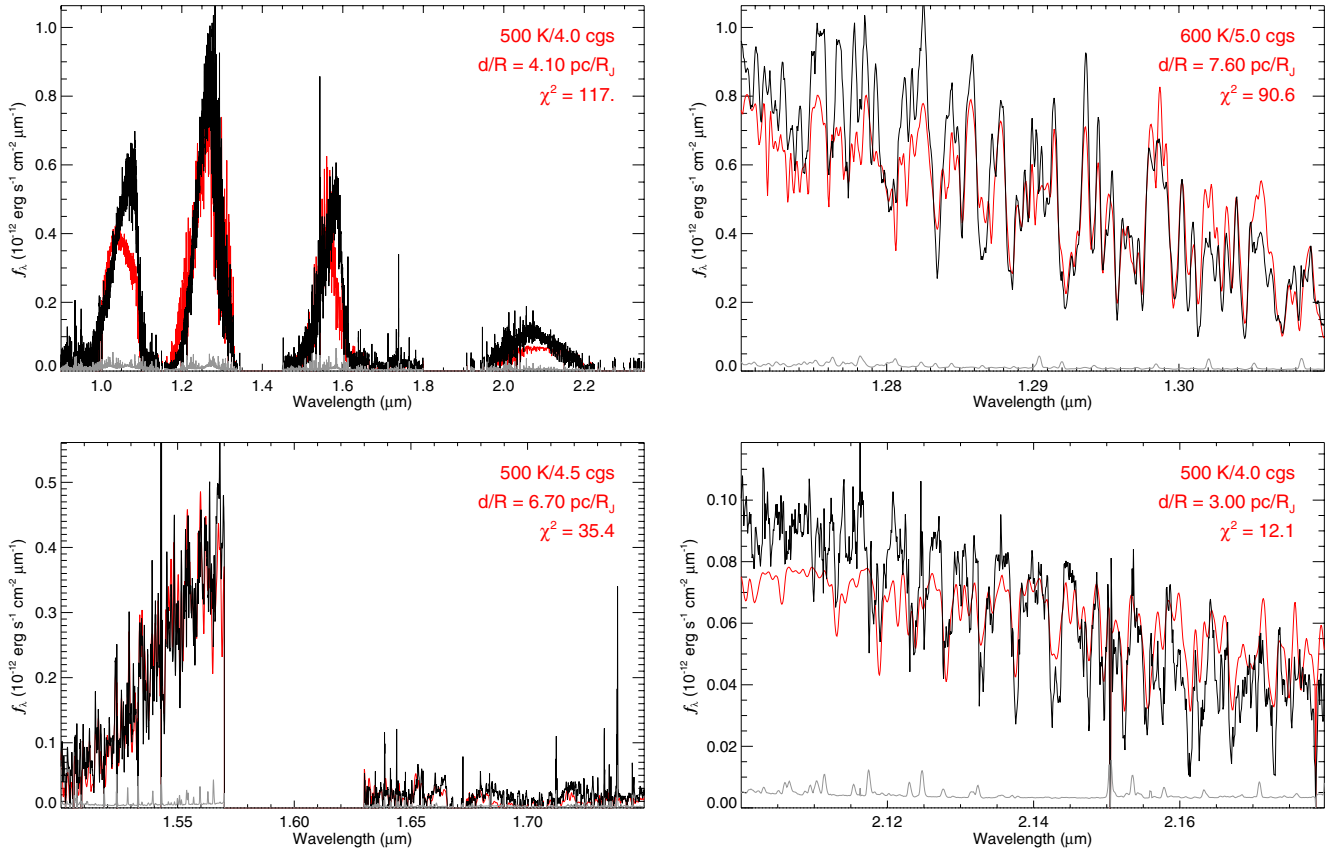


Figure 6. Shown are the best-fit model atmospheres (red) compared to the NIR spectrum of UGPS 0722–05 (black line) and error spectrum (gray line) for the entire spectrum (upper left panel), and narrow regions in the J band (upper right panel), H band (lower left panel), and K band (lower right panel) for the distance-restricted fits. The agreement between the best-fit model ($T = 500$ K, $\log g = 4.0$, $[m/H] = 0.0$) and the FIRE observations (upper left panel) is best near the J -band peak, but there are large deviations throughout the NIR regime. However, within restricted wavelength ranges (other panels) the agreement between the model and data improves.

(A color version of this figure is available in the online journal.)

Table 3
Atmosphere Model Measurements

Parameter	Full Spectrum	y	J	J_r	H	H_r	K	K_r
Fit Ranges (μ m)	0.9–2.35	0.9–1.15	1.15–1.35	1.27–1.31	1.45–1.8	1.50–1.57, 1.63–1.75	1.9–2.35	2.1–2.18
dof	3409	982	743	182	1016	585	659	220
No distance restriction								
Min χ^2	87.4	19.0	66.3	62.7	107	35.4	10.9	7.5
T_{eff} (K)	700 ± 50	750 ± 70	600 ± 50	620 ± 60	590 ± 60	500 ± 50	610 ± 60	630 ± 70
$\log g$ (cgs)	4.0 ± 0.3	3.5 ± 0.3	4.5 ± 0.3	4.5 ± 0.3	4.1 ± 0.4	4.4 ± 0.3	3.7 ± 0.4	3.8 ± 0.4
Mass (M_{\odot})	0.005	0.003	0.012	0.012	0.008	0.011	0.004	0.004
Age (Gyr)	0.08	0.02	0.9	0.9	0.5	1.5	0.07	0.09
d (pc)	49	61	22	20	27	6.4	23	24
Distance restriction								
Min χ^2	118	74.3	196	90.6	118	35.4	20.9	12.1
T_{eff} (K)	500 ± 50	500 ± 50	500 ± 50	600 ± 50	500 ± 50	500 ± 50	520 ± 70	510 ± 60
$\log g$ (cgs)	4.0 ± 0.3	4.0 ± 0.3	4.0 ± 0.3	5.0 ± 0.3	4.4 ± 0.3	4.4 ± 0.3	4.4 ± 0.5	4.2 ± 0.4
Mass (M_{\odot})	0.005	0.005	0.005	0.029	0.010	0.011	0.013	0.009
Age (Gyr)	0.2	0.2	0.3	5.1	1.3	1.4	2.1	1.0
d (pc)	4.6	4.2	4.9	6.7	6.2	6.4	4.2	3.5

the radial (± 50 km s $^{-1}$ in steps of 1.25 km s $^{-1}$ about the reported value) and rotational velocities (0–100 km s $^{-1}$ in steps of 3 km s $^{-1}$) of the model templates to find a χ^2 minimum. Means and uncertainties in the atmospheric parameters (T_{eff} , $\log g$) and associated physical parameters (mass, age, and radius based on the evolutionary models of Baraffe et al. 2003) were

determined using the F -test probability distribution function as a weighting factor, as described in Burgasser et al. (2010). We also propagated sampling uncertainties of 50 K and 0.25 dex for T_{eff} and $\log g$, respectively.

The best-fit models and data are plotted in Figure 6. The upper panel displays the best fit to the entire spectrum, with the

distance limit enforced. There are significant deviations between the model and data in the *JHK* bands, suggesting that there remain missing or incorrect molecular opacity in the BT-Settl model calculations. However, the agreement between the best-fit distance-restricted model and data improves in the “narrow” regions, as shown in Figure 6. Given the deviations between the models and data, caution is warranted in using the physical parameters listed in Table 3, however, some general trends do emerge. First, we examined the relative effect of the distance restriction. The distance-restricted fits prefer a cooler T_{eff} , ~ 500 K instead of 700 K. The distance-restricted fits also suggest a higher surface gravity and older age, but there is no clear behavior in the mass determination. We also note that most of the fits with unrestricted distances prefer distances much larger than the measured parallax.

We adopt the restricted distance and wavelength sets (J_r , H_r , and K_r) for further discussion. These clipped wavelength sets were chosen to sample strong molecular absorption, mostly due to CH_4 . Agreement between the data and model within these windows indicates that the BT-Settl models may have the proper opacity included in these windows, but due to the dearth of benchmark BDs (Konopacky et al. 2010, and references therein), the physical parameters derived from these fits may have large systematic uncertainties. These fits suggest an object with $T_{\text{eff}} \simeq 500\text{--}600$ K, $\log g \simeq 4.2\text{--}5.0$, mass $\sim 10\text{--}30 M_{\text{Jup}}$, and an age of 1–5 Gyr. These parameters agree with the results of Lucas et al. (2010), who reported $T_{\text{eff}} = 480\text{--}560$ K, $\log g = 4.0\text{--}4.5$, mass = 5–15 M_{Jup} , and an age of 0.2–2.0 Gyr. To examine the accuracy in other bandpasses, synthetic photometry was computed in the Infrared Array Camera and *WISE* bands reported in Table 1 using the $T_{\text{eff}} = 500$ K, $\log g = 4.0$ model and reported parallax. In general, the synthetic photometry matched the reported values within <1 mag, and agreed within <0.05 mag for the *W1* and *W3* bandpasses, suggesting the calculated opacities in these filters may be correct. We note that the H_r region produced identical results with and without the distance restriction, suggesting that the BT-Settl models may perform well in this wavelength range. However, adopting the uncertainties from the physical parameters from only this range probably underestimates the systematic errors, especially since only one set of models was considered.

4. CONCLUSIONS

We have presented an analysis of FIRE observations of one of the coldest BDs known, the T9 infrared spectral standard UGPS 0722–05.¹¹ Using current line lists and atmospheric models, we characterized the NIR SED and constrained the physical parameters of UGPS 0722–05. At the resolutions achieved with FIRE, we are able to identify individual molecular features throughout the spectrum. As more cold BDs are discovered through new surveys such as *WISE* (Wright et al. 2010), the Canada–France Brown Dwarf Survey (Albert et al. 2011) and VISTA (Irwin et al. 2004), these features may be useful for determining fundamental parameters and discriminating between spectral types. Unfortunately, the BT-Settl model atmospheres do not adequately reproduce the spectral features observed at these low temperatures across the NIR regime, although fits over restricted regions are more robust. By limiting our analysis to the wavelength and distance-restricted fits, we derive a T_{eff} of 500–600 K, $\log g$ of 4.2–5.0, mass of 10–30

M_{Jup} , and age of 1–5 Gyr. These values agree well with the results from Lucas et al. (2010), however, the data should be re-examined as models are further refined.

The RV of UGPS 0722–05 was measured as 46.9 km s^{-1} to a precision of a few km s^{-1} . Combined with parallax and proper motion measurements from Lucas et al. (2010), the Galactic orbit of UGPS 0722–05 was computed to investigate its parent population. Its orbit is similar to many thin disk objects, exhibiting low eccentricity and vertical excursions taking it only ~ 60 pc away from the plane. This orbit also agrees well with the age of 1–5 Gyr derived from the atmospheric fits. As larger catalogs of cold BDs with well-measured kinematic properties are assembled, their ensemble properties will be important for testing the predictions of Milky Way kinematic structure models (i.e., Roškar et al. 2008; Loebman et al. 2011).

The rotational velocity of UGPS 0722–05 was also measured, employing the BT-Settl atmospheric model as a template. The object is rotating at $\sim 40 \pm 10 \text{ km s}^{-1}$, similar to other late-type L and T dwarfs and further evidence that rotational braking is not efficient in BDs (Zapatero Osorio et al. 2006; Reiners & Basri 2008). In future investigations, we will secure observations of BDs with small projected rotational velocities such as SDSSJ134646.45–003150.4 (Zapatero Osorio et al. 2006) to serve as empirical templates.

We thank the entire Magellan and Las Campanas staff for their support and guidance during the assembly, installation, and commissioning of FIRE. We especially thank our telescope operator during commissioning, Mauricio Martinez. FIRE was constructed with support from the NSF/MRI grant AST-0649190 and Curtis Marble. J.J.B. acknowledges the financial support of NSF grant AST-0544588. J.J.B. thanks Sergey Yurchenko and Bob Barber for assistance with line lists and Robyn Sander-son for enlightening conversations on Galactic orbits. R.A.S. acknowledges the financial and corporal support of the A.J.B. chair. We thank the anonymous referee for comments which greatly improved the clarity and content of this manuscript.

Facility: Magellan:Baade

REFERENCES

- Albert, L., Artigau, É., Delorme, P., et al. 2011, *AJ*, **141**, 203
- Allard, F., Guillot, T., Ludwig, H.-G., et al. 2003, in IAU Symp. 211, Brown Dwarfs, ed. E. Martín (San Francisco, CA: ASP), 325
- Allard, F., Homeier, D., & Freytag, B. 2010, arXiv:1011.5405
- Asplund, M., Grevesse, N., Sauval, A. J., & Scott, P. 2009, *ARA&A*, **47**, 481
- Baraffe, I., Chabrier, G., Barman, T. S., Allard, F., & Hauschildt, P. H. 2003, *A&A*, **402**, 701
- Barber, R. J., Tennyson, J., Harris, G. J., & Tolchenov, R. N. 2006, *MNRAS*, **368**, 1087
- Basri, G., & Martín, E. L. 1999, *AJ*, **118**, 2460
- Berger, E. 2006, *ApJ*, **648**, 629
- Burgasser, A. J., Hennawi, J. F., Simcoe, R. A., et al. 2009, *PASP*, **121**, 1409
- Bochanski, J. J., Munn, J. A., Hawley, S. L., et al. 2007, *AJ*, **134**, 2418
- Bouvier, J., Forestini, M., & Allain, S. 1997, *A&A*, **326**, 1023
- Bowler, B. P., Liu, M. C., & Cushing, M. C. 2009, *ApJ*, **706**, 1114
- Browning, M. K. 2008, *ApJ*, **676**, 1262
- Browning, M. K., Basri, G., Marcy, G. W., West, A. A., & Zhang, J. 2010, *AJ*, **139**, 504
- Burgasser, A. J. 2004, *ApJS*, **155**, 191
- Burgasser, A. J., Simcoe, R. A., Bochanski, J. J., et al. 2010, *ApJ*, **725**, 1405
- Burningham, B., Pinfield, D. J., Lucas, P. W., et al. 2010, *MNRAS*, **406**, 1885
- Burrows, A., Hubbard, W. B., Lunine, J. I., & Liebert, J. 2001, *Rev. Mod. Phys.*, **73**, 719
- Burrows, A., Marley, M., Hubbard, W. B., et al. 1997, *ApJ*, **491**, 856
- Chen, B., Stoughton, C., Smith, J. A., et al. 2001, *ApJ*, **553**, 184
- Cushing, M. A., Kirkpatrick, J. D., Gellino, C. R., et al. 2011, arXiv:1108.4678
- Cushing, M. C., Marley, M. S., Saumon, D., et al. 2008, *ApJ*, **678**, 1372

¹¹ The FIRE spectrum is available online at <http://personal.psu.edu/jjb29/0722.html>.

- Cushing, M. C., Vacca, W. D., & Rayner, J. T. 2004, *PASP*, **116**, 362
- Dauphole, B., & Colin, J. 1995, *A&A*, **300**, 117
- Fink, U., & Larson, H. P. 1979, *ApJ*, **233**, 1021
- Freytag, B., Allard, F., Ludwig, H.-G., Homeier, D., & Steffen, M. 2010, *A&A*, **513**, A19
- Golimowski, D. A., Leggett, S. K., Marley, M. S., et al. 2004, *AJ*, **127**, 3516
- Gray, D. F. (ed.) 1992, *The Observation and Analysis of Stellar Photospheres* (Cambridge: Cambridge Univ. Press)
- Hallinan, G., Antonova, A., Doyle, J. G., et al. 2008, *ApJ*, **684**, 644
- Hauschildt, P. H., Allard, F., Ferguson, J., Baron, E., & Alexander, D. R. 1999, *ApJ*, **525**, 871
- Horne, K. 1986, *PASP*, **98**, 609
- Irwin, M. J., Lewis, J., Hodgkin, S., et al. 2004, *Proc. SPIE*, **5493**, 411
- Johnson, D. R. H., & Soderblom, D. R. 1987, *AJ*, **93**, 864
- Jurić, M., Ivezić, Ž., Brooks, A., et al. 2008, *ApJ*, **673**, 864
- Kelson, D. D. 2003, *PASP*, **115**, 688
- Kerr, F. J., & Lynden-Bell, D. 1986, *MNRAS*, **221**, 1023
- Kirkpatrick, J. D., Cushing, M. C., Gelino, C. R., et al. 2011, arXiv:1108.4677
- Konopacky, Q. M., Ghez, A. M., Barman, T. S., et al. 2010, *ApJ*, **711**, 1087
- Kuzmin, G. 1956, *AZh*, **33**, 27
- Lawrence, A., Warren, S. J., Almaini, O., et al. 2007, *MNRAS*, **379**, 1599
- Leggett, S. K., Marley, M. S., Freedman, R., et al. 2007, *ApJ*, **667**, 537
- Loebman, S. R., Roškar, R., Debattista, V. P., et al. 2011, *ApJ*, **737**, 8
- Lucas, P. W., Tinney, C. G., Burningham, B., et al. 2010, *MNRAS*, **408**, L56
- Macintosh, B., Graham, J., Palmer, D., et al. 2006, *Proc. SPIE*, **6272**, 62720
- Marshall, J. L., Burles, S., Thompson, I. B., et al. 2008, *Proc. SPIE*, **7014**, 701454
- Metchev, S. A., Kirkpatrick, J. D., Berriman, G. B., &Looper, D. 2008, *ApJ*, **676**, 1281
- Miyamoto, M., & Nagai, R. 1975, *PASJ*, **27**, 533
- Mohanty, S., & Basri, G. 2003, *ApJ*, **583**, 451
- Nassar, R., & Bernath, P. 2003, *J. Quant. Spectrosc. Radiat. Transfer*, **82**, 279
- Reid, I. N., & Mahoney, S. 2000, *MNRAS*, **316**, 827
- Reiners, A., & Basri, G. 2008, *ApJ*, **684**, 1390
- Rothman, L. S., Gordon, I. E., Barbe, A., et al. 2009, *J. Quant. Spectrosc. Radiat. Transfer*, **110**, 533
- Roškar, R., Debattista, V. P., Quinn, T. R., Stinson, G. S., & Wadsley, J. 2008, *ApJ*, **684**, L79
- Saumon, D., Marley, M. S., Cushing, M. C., et al. 2006, *ApJ*, **647**, 552
- Schönrich, R., Binney, J., & Dehnen, W. 2010, *MNRAS*, **403**, 1829
- Simcoe, R. A., Burgasser, A. J., Bernstein, R. A., et al. 2008, *Proc. SPIE*, **7014**, 70140
- Simcoe, R. A., Burgasser, A. J., Bochanski, J. J., et al. 2010, *Proc. SPIE*, **7735**, 773514
- Skumanich, A. 1972, *ApJ*, **171**, 565
- Vacca, W. D., Cushing, M. C., & Rayner, J. T. 2003, *PASP*, **115**, 389
- West, A. A., & Basri, G. 2009, *ApJ*, **693**, 1283
- Wright, E. L., Eisenhardt, P. R. M., Mainzer, A. K., et al. 2010, *AJ*, **140**, 1868
- Yurchenko, S. N., Barber, R. J., & Tennyson, J. 2011, *MNRAS*, **413**, 1828
- Zapatero Osorio, M. R., Martín, E. L., Béjar, V. J. S., et al. 2007, *ApJ*, **666**, 1205
- Zapatero Osorio, M. R., Martín, E. L., Bouy, H., et al. 2006, *ApJ*, **647**, 1405